APPLICATION OF FINITE ELEMENT METHOD TO FRACTURE MECHANICS

H. MIYAMOTO,

The Faculty of Engineering, University of Tokyo, Tokyo, Japan

ABSTRACT

This paper shows some examples in which the finite element method has been applied successfully to the fracture mechanics. First the stress intensity factor of the semi-elliptical surface flaw in a rectangular plate is obtained by the crack opening displacement. Secondarily elastic-plastic behavior near the tip of double edged cracks in a rectangular plate is analyzed three-dimensionally and the difference between the state of stress in the center plane and the surface of the plate is discussed. Further two-dimensional analysis of the cracked plate under cyclic loadings is carried out and the alternating plastic zone and the deformation of the crack surface are obtained. The above analyses are treated for the homogeneous and isotropic body. Next inhomogeneity due to crystal grains is considered. Coarse grained aluminum sheet under tension is analyzed considering the orientation of each grain and the initiation of the slip lines is estimated. The results agreed well with the experiment. At last the above method is combined with the Monte-Carlo method and Young's modulus and Poisson's ratio are obtained.

1. INTRODUCTION

The study about the mechanism of the fracture will be called "Fracture Mechanics (F.M.)" (in wider sense)*. The research about the fracture mechanics in the past, present and future will be classified into three categories: (Fig. 1)

(1) Macroscopic Fracture Mechanics
(2) Microscopic Fracture Mechanics
(3) Atomistic Fracture Mechanics

---

* The term "Fracture Mechanics" used in U.S.A. is concerned mainly with "Linear Fracture Mechanics" in two-dimensional theory of elasticity. In this paper the term "Fracture Mechanics" will be used in wider sense.

By Macroscopic F.M. we mean the isotropic and homogeneous linear and non-linear F.M. in two- and three-dimensional problem. It includes the case of monotonic and cyclic loading. By Microscopic F.M. we mean the fracture mechanics of metals interpreted in terms of crystal grains. By our experiment [1] the dimension of the plastic zone at the tip of a crack in the carbon steel is under 0.01 mm and it corresponds to that of crystal grains. So it is not proper to assume that the metal is isotropic and homogeneous and here is the necessity to treat these problems by the anisotropic and heterogeneous continuum mechanics. By Atomistic fracture mechanics we mean the F.M. in the atomic order and in this category the behaviors of dislocations will be one of the main problem but this category will not be discussed in this paper. Among these the future problems of the F.M. from the standpoint of the continuum mechanics are considered to be three-dimensional linear fracture mechanics, non-linear fracture mechanics and microscopic fracture mechanics and to solve these problems the finite element method is very powerful and probably an only approach which we have at present.

In this paper we describe the results of the application of the finite element method to fracture mechanics which were obtained in our laboratory.

2. STRESS INTENSITY FACTOR OF THE SEMI-ELLIPTICAL SURFACE FLAW IN TENSION PLATE [2]

2.1. Analysis of Stress Intensity Factor by the Finite Element Method

In two-dimensional problems there are many analytical solutions of the stress intensity factor, but those in three-dimensional problems are difficult to obtain analytically. However, when the mode of stress near the crack tip is known, the stress intensity factor is obtained numerically by using following equation.

$$K_I = \sqrt{\pi}\,\frac{E}{2(1-\nu^2)}\,\frac{w(r)}{\sqrt{2r}} \qquad \text{(in case of plane strain)} \qquad (1)$$

where w(r) is the crack opening displacement and r is the normal inward distance from the crack tip. This chapter describes the finite element analysis of the stress intensity factor for a surface flawed tension plate shown in Fig. 2. The approximate solutions of this problem have been obtained by Irwin [3] and Kobayashi [4] and the numerical results of this analysis are compared with these results.

2.2. Problem Specifications

Calculations are carried out in three cases (1) a/t=0.8, a/2c=0.3 (2) a/t=0.8, a/2c=0.1 (3) a/t=0.3, a/2c=0.1 . The width of a plate is b=6c and the plate height is h=4c. Material constants are as follows: Young's modulus, E , kg/mm^2 ..... 21000, Poisson's ratio, ν ..... 0.3 The calculations are carried out on one-quarter of the specimen due to the symmetry of the problem.

2.3. Step Method [5], [6]

In three-dimensional problem a large number of elements must be used to obtain a reasonable solution. So, the step method is used taking account the computational time and the capacity of the computer. At first (STEP 1), using the coarse mesh (Fig. 3a), the solution is obtained. Next (STEP 2), using nodal force distributions as load conditions the solution near the crack tip is obtained more accurately, (Fig. 3b).

2.4. Results

Fig. 4 shows the order of stress singularity near the crack tip. From this figure it is observed that the stress singularity is $r^{-\frac{1}{2}}$ at $\theta \neq 0^\circ$ and is not $r^{-\frac{1}{2}}$ at $\theta = 0^\circ$. Fig. 5 shows the crack opening displacement. The relation between the crack opening displacement and the distance from the crack tip is shown in Fig. 6. The crack opening displacement is proportional to $r^{\frac{1}{2}}$ at $\theta \neq 0^\circ$ and not proportional to $r^{\frac{1}{2}}$ at $\theta = 0^\circ$. The stress intensity factor is calculated from the crack opening displacement at 2~4 nodal points away from the crack tip using the eq. (1). Fig. 7 represents the variation of the stress intensity magnification factor $M_e = (K_I)_{max} / K_{IO}$ along the crack border, where K_{IO} is the maximum stress intensity factor of the embedded elliptical crack of same geometry. The result in terms of M_e is presented in Table 1. Irwin's result $M_e = 1.10$ is proper when $a/t = 0.3$ but smaller when $a/t = 0.8$. Kobayashi's result agrees well with our result but is smaller than ours. There are three approximations in his theory and these can be clarified by the comparison with the more extensive result by the finite element method.

3. THREE-DIMENSIONAL ANALYSIS OF THE ELASTIC-PLASTIC RESPONSE AT THE CRACK TIP UNDER MONOTONIC LOADING [7]

3.1. Application of the Finite Element Method to the Incremental Theory of Plasticity [8]

Elastic-plastic problem can be analyzed similarly to the elastic ones by the finite element method. The difference between them is as follows:

(1) The plastic stress-strain matrix $[D^p]$ is used instead of elastic one $[D^e]$ for the yielded elements.

(2) The load increments ΔP is chosen such that the yielding of element occurs one by one. And the stress increments $\Delta\sigma_{ij}$ and strain increments $\Delta\varepsilon_{ij}$ caused by ΔP are calculated at each stage.

Details of the above procedures are described in the literature [8]. The explicit form of $[D^p]$ in three-dimensional problem is as follows:

$$[D^p] = \frac{E}{1+\nu}\begin{bmatrix} (1-\nu)/(1-2\nu)-\delta_x'^2/S_o & & & & \\ \nu/(1-2\nu)-\delta_x'\delta_y'/S_o & (1-\nu)/(1-2\nu)-\delta_y'^2/S_o & & \text{SYM.} & \\ \nu/(1-2\nu)-\delta_x'\delta_z'/S_o & \nu/(1-2\nu)-\delta_y'\delta_z'/S_o & (1-\nu)/(1-2\nu)-\delta_z'^2/S_o & & \\ -\delta_x'\tau_{yz}/S_o & -\delta_y'\tau_{yz}/S_o & -\delta_z'\tau_{yz}/S_o & \frac{1}{2}-\tau_{yz}^2/S_o & \\ -\delta_x'\tau_{zx}/S_o & -\delta_y'\tau_{zx}/S_o & -\delta_z'\tau_{zx}/S_o & -\tau_{yz}\tau_{zx}/S_o & \frac{1}{2}-\tau_{zx}^2/S_o \\ -\delta_x'\tau_{xy}/S_o & -\delta_y'\tau_{xy}/S_o & -\delta_z'\tau_{xy}/S_o & -\tau_{yz}\tau_{xy}/S_o & -\tau_{zx}\tau_{xy}/S_o \quad \frac{1}{2}-\tau_{xy}^2/S_o \end{bmatrix} \tag{2}$$

$$S_o = 2\bar{\sigma}^2(G+H'/3)/3G$$

3.2. Problem Specifications

The geometry of the specimen is shown in Fig. 8. The width of a plate is b, length 8b/3, plate thickness b/5 and the crack length is c=b/6.

Material constans are as follows:

Young's modulus, E , Kg/mm^2 ..... 7200 , Poisson's ratio, ν , ...0.34

Uniaxial yield stress, σ_Y , Kg/mm^2 .....3.0

Strain hardening rate, $H' = d\bar{\sigma} / d\bar{\varepsilon}^p$, Kg/mm^2 .....68.2

The three-dimensional analysis is carried out for only a portion of the specimen shown in Fig. 9. The load condition on y=b/5 is then calculated from the nodal force distribution in plane stress analysis.

3.3. Results

The elastic stress ahead of the crack and normal to it is shown in Fig. 10 for the center of the plate (z=0) and for the surface (z=b/10). The variation of the stresses through the thickness of the plate is illustrated in Fig. 11 and compared with the plane stress values calculated in the two-dimensional example. The first element yields at an applied gross tension of $0.296\,\sigma_Y$. Fig. 12 shows the growth of the plastic zone ahead of the crack in the plane of the crack. This figure shows that the plastic zone is smaller at the center side of the plate than at the surface side. The growth of the plastic zone normal to the crack at the center of the plate (z=0) and at the surface (z=b/10) is shown in Figs. 13 and 14, respectively. Above results represent that the stress normal to the crack is higher and the plastic zone is smaller at the center at the surface, so the fracture toughness is larger at the surface. This results coincides with that the crack propagates faster at the center side of the plate.

4. TWO-DIMENSIONAL ANALYSIS OF THE ELASTIC-PLASTIC RESPONSE AT THE CRACK TIP UNDER CYCLIC LOADING [9]

When one wants to study the mechanism of the fatigue crack propagation, it is essential to make clear the elastic-plastic behavior near the crack tip under cyclic loadings. This chapter shows some examples in which the incremental method is applied to the crack problem for cyclic loadings.

As the test problem, a smooth rectangular plate has been applied completely reversed tension-compression load. The hysteresis curve obtained by the calculation is shown in Fig. 15. In the diagram $\overrightarrow{OA}$ corresponds to the original elastic loading. All the elements yield at the same time at A, then plastic flow accompanied by the strain hardening occurs along $\overrightarrow{AB}$. B is the point of the tensile peak load. Next when the tensile load is removed and compressive load is applied, the plate behave elastically at first along $\overrightarrow{BC}$, then the reversed plastic flow occurs along $\overrightarrow{CD}$. The criterion of reyielding at C is such that the equivalent stress at C is equal to the one at B. No Bauschinger effect has

been considered. When the compressive load is removed and tensile load is applied, the plate behave elastically at first along DE, and so forth.

The first example is the internal crack under pulsating tensile stress. The shape of the specimen is shown in Fig. 16. Fig. 17 shows the distribution of σ_y and ε_y ahead of the crack tip.(a=1.0 mm, L=0 — 550 Kg). At the tensile peak load (loading), the plastic zone spread about 0.3 mm from the crack tip. When the load is completely removed (unloading), some element very near the crack tip (about 0.06 mm) yield again by the compressive residual stress. The region near the crack tip, then, can be classified three domains illustrated in Fig. 18, that is, (1) the surrounding elastic region, (2) the region which yields for the first peak load but behaves elastically for the following loading cycle, and (3) the region which reyields by the compressive residual stress and forms hysteresis loop. Fatigue damage is considered to accumulate in the region (3), which is important to the fatigue crack propagation. The region (2) and (3) varies with crack length as shown in Fig. 19 when the tensile peak load is held constant. And the area of each region, S_p and S_p', is proportional to K^4 where K is the stress intensity factor of these cracks (Fig. 20). Fig. 21 shows the crack opening displacement at the tensile peak load and zero load. No crack closing is observed.

Next a notched specimen with cracks under completely reversed stress is analyzed. The main difficulty of the problem is the crack closing at the compressive cycle. This difficulty can be solved by the incremental method. Joints on the crack surface are regarded to be closed when the normal displacement of these joints become to zero. And the closed joints are fixed one by one for the following stage (Fig. 23a). Three cases in Fig. 22 are treated. Fig. 23b shows the alternating plastic zone and deformation of the crack surface according to the loading cycle (case C, a=1.0 mm, L=50.0 Kg). Fig. 24 shows the distribution of ε_y ahead of the crack tip at tensile and compressive peak load. A, B, and C denote the cases in Fig. 22.

5. INITIATION OF SLIP LINES IN THE COARSE GRAINED SPECIMEN OF PURE ALUMINUM [10]

5.1. Simulation Techniques by the Finite Element Method

In this analysis the following assumptions are made:

(1) The grain boundary is the one at which only the orientation of two adjacent grains are different.

(2) In a grain, the material is homogeneous (the defects are not considered).

The local coordinates are given in eq. (3). (Fig. 25)

$$\begin{Bmatrix} x' \\ y' \\ z' \end{Bmatrix} = \begin{bmatrix} l_1 & m_1 & n_1 \\ l_2 & m_2 & n_2 \\ l_3 & m_3 & n_3 \end{bmatrix} \begin{Bmatrix} x \\ y \\ z \end{Bmatrix} \qquad (3)$$

The relation between the stress σ and strain ε in the global coordinate system of a triangular prism element is as follows:

$$\{\sigma\} = [\Phi]^T [C^e][\Phi]\{\varepsilon\} = [D^e]\{\varepsilon\} \tag{4}$$

$[\Phi]$: transformation matrix of strain

$[C^e]$: elastic modulus

In eq. (4)

The matrix $[D^e]$ in eq. (5) is called as the stress- strain matrix. If N is the number of the triangular prism element used in the analysis. 12N is the number of the slip systems and the resolved shear stress.* Considering that the slip line initially appears at the location where the resolved shear stress is maximum, the location where the slip line initially appears is the element of the maximum resolved shear stress. Once the element and the slip plane of the maximum resolved shear stress are obtained, the angle between the x axis of the specimen and the slip line is calculated as follows:(Fig. 26)

$$\theta = \tan^{-1}\left(-\frac{l_1 + l_2 + l_3}{m_1 + m_2 + m_3}\right) \qquad \theta = \tan^{-1}\left(-\frac{-l_1 + l_2 + l_3}{-m_1 + m_2 + m_3}\right)$$

(slip plane of the quadrant I) (slip plane of the quadrant II)

$$\theta = \tan^{-1}\left(-\frac{-l_1 - l_2 + l_3}{-m_1 - m_2 + m_3}\right) \qquad \theta = \tan^{-1}\left(-\frac{l_1 - l_2 + l_3}{m_1 - m_2 + m_3}\right) \tag{5}$$

(slip plane of the quadrant III) (slip plane of the quadrantIV)

5.2. Experiment

The testpiece used in this analysis is the one of pure Al (99.99%). The back Laue method is used to determine the orientation of the grain. By this measurement, the components of the matrix in eq. (3) are determined.

5.3. Problem Specifications

Fig. 27 shows the coarse grained specimens of pure Al. Fig. 28 shows the sketch of the specimen and the numbers in this figure shows the grains. In Fig. 28 also the slip lines are illustrated. The photograph of the slip lines in Fig. 28 is shown in Fig. 29 and the angle between the x axis of the specimen and the slip lines is 107.0°.

In the analysis, only the part between the dashed lines in Fig. 28 is considered and divided into the triangular prism element illustrated in Fig. 30.

5.4. Results

Figs. 31 and 32 show the distribution of σ_x and ε_x. From Fig. 32 the deformation in the grains is not uniform. In Table 2 the comparison between the analytical and experimental results is shown. There is good agreement between the analytical and experimental results.

---

* In this analysis FCC metals such as Al are considered.

6. DETERMINATION OF ELASTIC CONSTANTS OF POLYCRYSTALLINEE METAL [10]

In this chapter the estimation of the mechanical properties of a polycrystal is tried by means of the probabilistic model. This is done by the combination of the finite element method and the Monte-Carlo method. Young's modulus and Poisson's ratio are calculated. The tension plate is composed of several layers of hexagonal cylinders which are considered as crystal grain (Fig.33 and Fig. 34). The orientation is constant in each grain, but random among each other. A hexagonal cylinder is divided into six triangular cylinder (Fig.34), and each of them is considered as the composite element of the finite element method. In this case the effect of grain boundaries are neglected. The method of stress and strain analysis is similar to the previous chapter.

The calculation is carried out on the aluminum specimen (12 mm×27.7 mm×2 mm) in longitudinal tension (10 Kg/mm^2). The breakdown along the thickness is one layer and total number of triangular cylinders and nodes are 56 and 80, respectively (Fig. 35). The elastic constants c_{ij} of the aluminum single crystal is

$$c_{11}=11020\ Kg/mm^2, \quad c_{12}=6330\ Kg/mm^2, \quad c_{44}=2855\ Kg/mm^2$$

The results is shown in Table 3. Young's modulus E is given as

$$E=(\ TENS\ )\ /\ (\ \Delta L/L)=7101.8\ Kg/mm^2$$

where (TENS) is uniform tension. The results agreed well with the handbook data, where E=7200 kg/mm^2 and $\nu=0.34$.

7. Summary

This paper describes some results of the application of the finite element method to the fracture mechanics. At present these results can be obtained only by the finite element method. The results are as follows:

(1) The stress intensity factor K_I of the semi-elliptical surface flaw is obtained using three-dimensional finite element method. The results coincides well with those of the previous calculations.

(2) The elastic-plastic response at the tip of the crack is obtained three-dimensionally in monotonic loading and the shape of elastic-plastic boundary is clarified. It coincides that due to Liu's estimation.

(3) The elastic-plastic response at the tip of the crack in cyclic loading is obtained and it is shown that the plastic region in cyclic loading is different from those in monotonic loading.

(4) The analysis of the mechanical behavior of the polycrystalline metal accounting for the grains is first succeeded and the stresses and strain in the grains are obtained. The location and direction of slip lines are coincided well between the calculations and experiments.

(5) The interpretation of Young's modulus and Poisson's ratio of polycrystalline metal by those of crystal grains is succeeded using the finite element and Monte-Carlo method.

REFERENCES

1 MIYAMOTO, H., SHIRATORI, M., "On the Strain near the Tip of a Fatigue Crack in Notched Steel Plates", J. Faculty Engng. Univ. Tokyo (B),29-4 (1968), 323.

2 MIYAMOTO, H., MIYOSHI, T., "Analysis of Stress Intensity Factor for Surface-Flawed Tension Plate", IUTAM Symposium, Liège (1970).

3 IRWIN, G. R., "Crack Extension Force for a Part-through Crack in a Plate", J. App. Mech., Trans. ASME, 29, E (1962).

4 KOBAYASHI, A. S., MOSS, W. L., "Stress Intensity Magnification Factors for Surface-Flawed Tension Plate and Notched Round Bar", Proc. of 2nd ICF, Brighton, England (1969).

5 PAULLING, J. L., "Application of the Finite Element Method to Ship Structural Analysis", Proc. of Japan-U.S. Seminar on Matrix Methods of Structural Analysis and Design, Tokyo (1969).

6 ANDO, Y., et. al., "Stress Analysis of the Cylindrical Shell with the Rectangular Cut-out", Preprint of 46th Congress of JSME, 212 (1969). (in Japanese)

7 MIYAMOTO, H., et. al., "Analysis of Stress and Strain Distribution at the Crack Tip by Finite Element Method", Proc. of Japan-U.S. Seminar on Matrix Methods of Structural Analysis and Design, Tokyo (1969).

8 YAMADA, Y., et. al., Int. J. Mech. Sci., 10-5 (1968).

9 MIYAMOTO, H., et al., "The Application of the Finite Element Method to the Fracture Mechanics", J. Faculty Engng. Univ. Tokyo (B), 31-1 (1971). (tobe published)

10 MIYAMOTO, H., et. al., "Interpretation of Mechanical Properties of Metals in terms of Microstructures", Bulletin of the JSME, 14-75 (1971). (to be published)

Table 1 Stress intensity magnification factor M_e

STRESS INTENSITY MAGNIFICATION FACTOR M_e

a/t	0.8	0.8	0.3
a/2c	0.1	0.3	0.1
F.E.M.	1.36	1.27	1.11
Irwin	1.10	1.10	1.10
Kobayashi	1.28	1.17	1.11

Table 2 Comparison between analytical and experimental results

		The location of first slip lines	The angle between the x axis and slip lines
NO.1	Simulation by the finite element method	Element NO. 207 in Figure 12	109.2°
	Experiment	Element NO. 207 in Figure 12	107.0°
NO.2	Simulation by the finite element method	Element NO. 228 in Figure 13	44.5°
	Experiment	Element NO. 228 in Figure 13	41.0°

Table 3 Distribution of ν_x , ν_z and σ_y / ε_y among grains

要素番号	$\nu_x = -\frac{\varepsilon_x}{\varepsilon_y}$	$\nu_z = -\frac{\varepsilon_z}{\varepsilon_y}$	$\frac{\sigma_y}{\varepsilon_y}$
1	0.363 32	0.355 58	7 096.0
3	0.366 62	0.337 39	7 221.9
6	0.337 38	0.346 07	7 287.6
8	0.333 41	0.338 11	7 526.0
13	0.356 83	0.343 01	6 732.3
17	0.357 06	0.344 75	6 937.3
22	0.385 97	0.349 06	7 191.5
27	0.344 75	0.351 71	6 670.5
31	0.363 49	0.355 29	7 373.4
36	0.354 38	0.357 56	6 732.8
41	0.335 91	0.336 06	6 860.3
45	0.358 11	0.330 18	7 239.4
50	0.400 22	0.324 04	7 237.8
55	0.340 65	0.348 65	7 283.8
MEAN VALUE	0.357 01	0.344 10	7 099.3

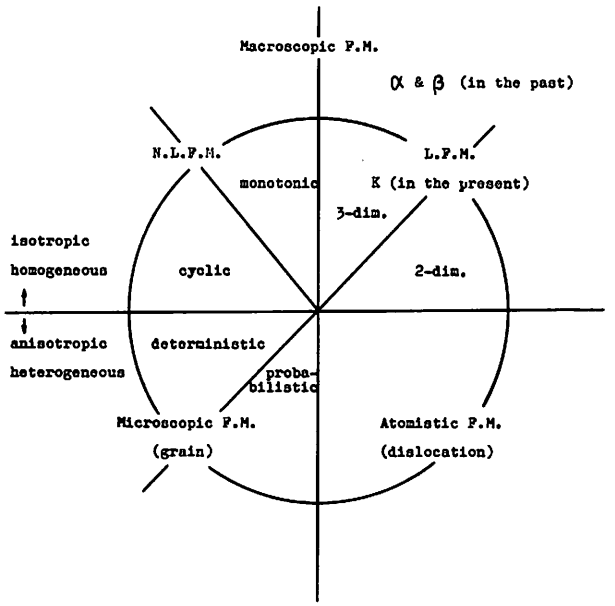

Fig. 1 Classification of the fracture mechanics

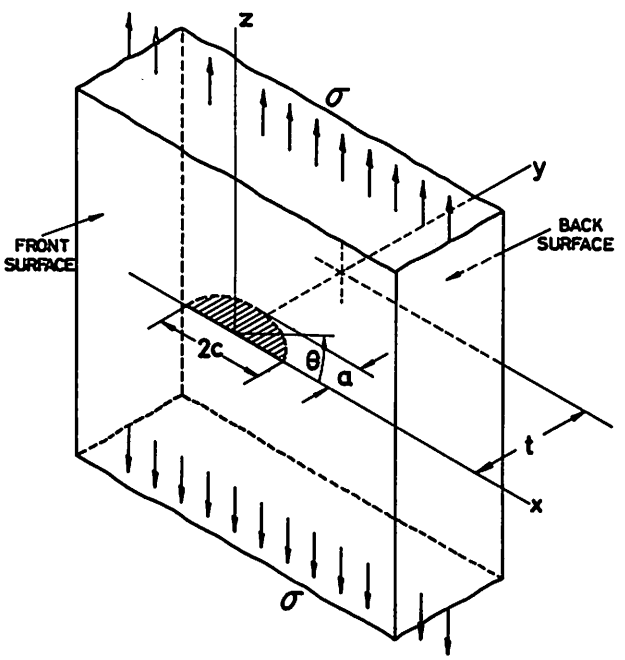

Fig. 2 Semi-elliptical surface flaw in a plate subjected to tension

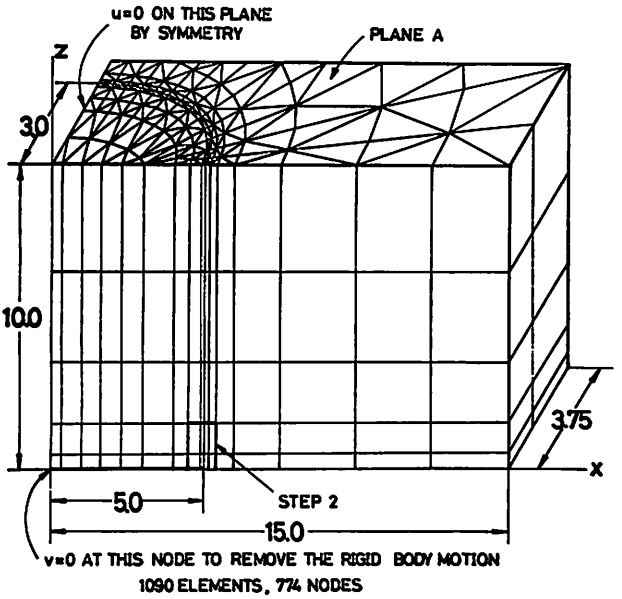

Fig. 3a Finte element representation of a semi-elliptical surface flaw (a/t=0.8, a/2c=0.3) —— coarse mesh (774 nodal points, 1090 elements)

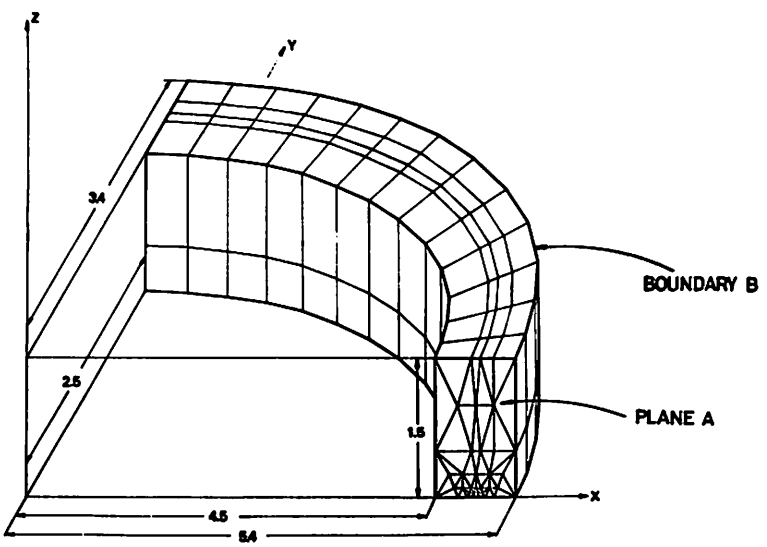

Fig. 3b Finite element representation of a semi-elliptical surface flaw (a/t=0.8, a/2c=0.3) —— fine mesh (574 nodal points, 793 elements)

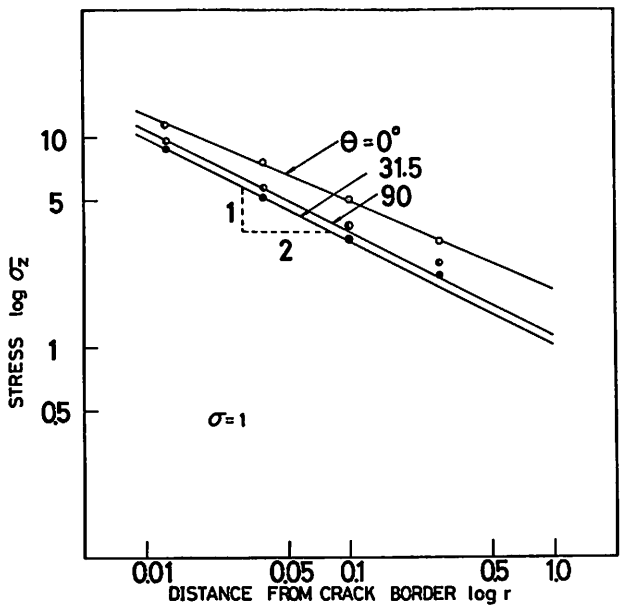

Fig. 4 The order of stress singularity near the crack tip

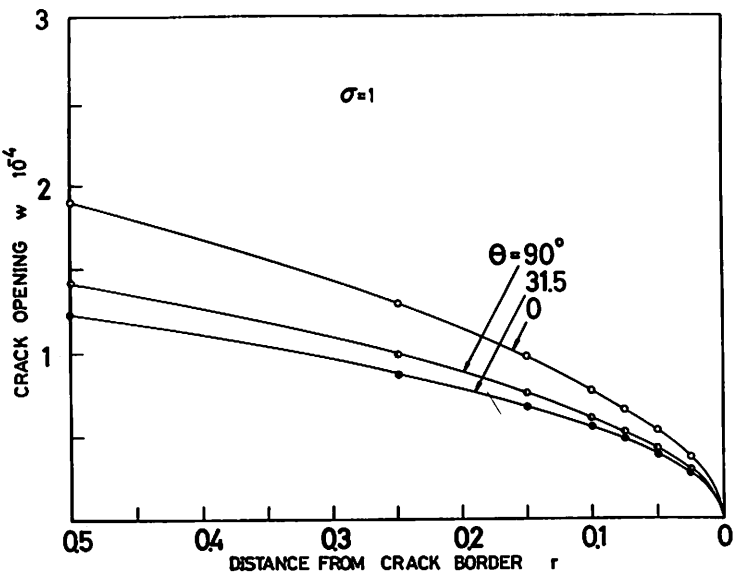

Fig. 5 The crack opening displacement

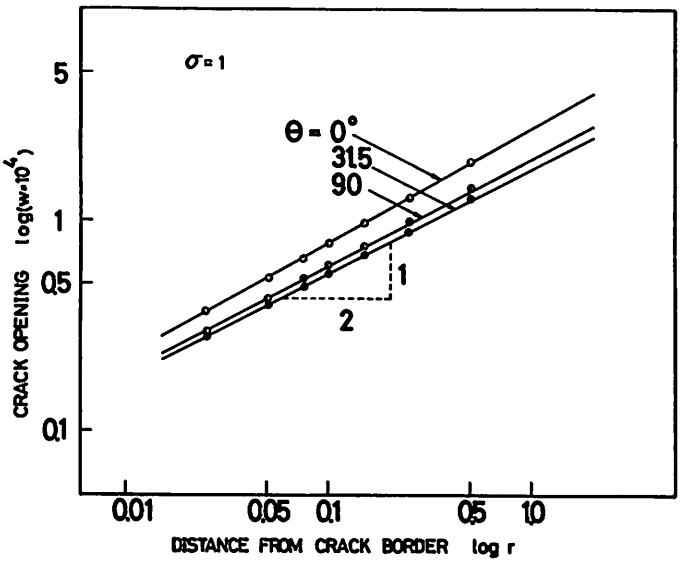

Fig. 6 The relation between the crack opening displacement and the distance from the crack tip

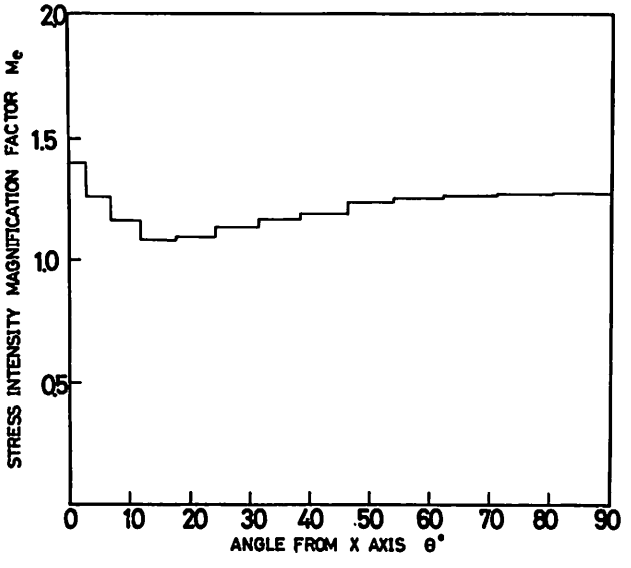

Fig. 7 The variation of the stress intensity magnification factor along the crack border

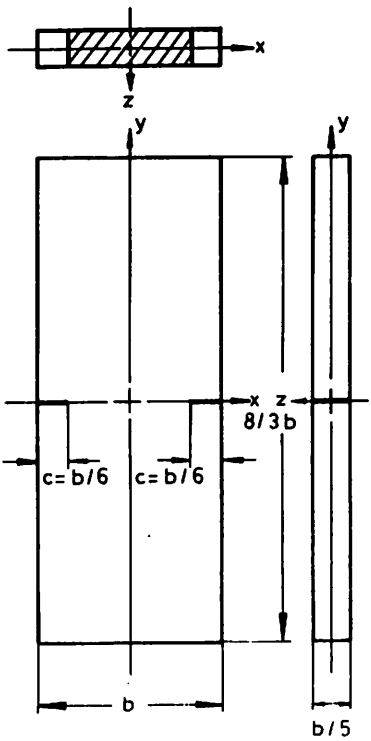

Fig. 8 Geometry of the specimen

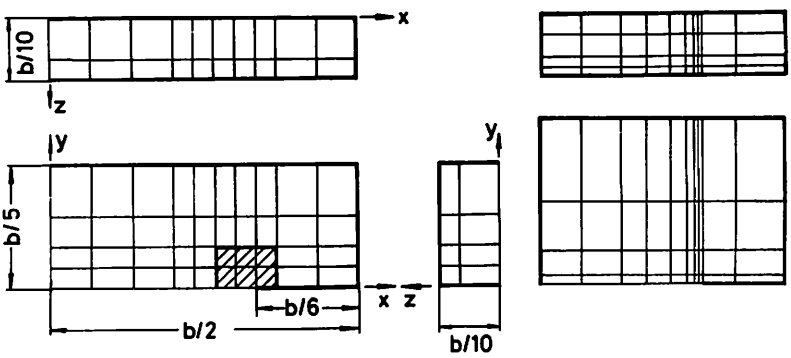

Fig. 9 Nodal breakdown on one-eighth of the rectangular crack example

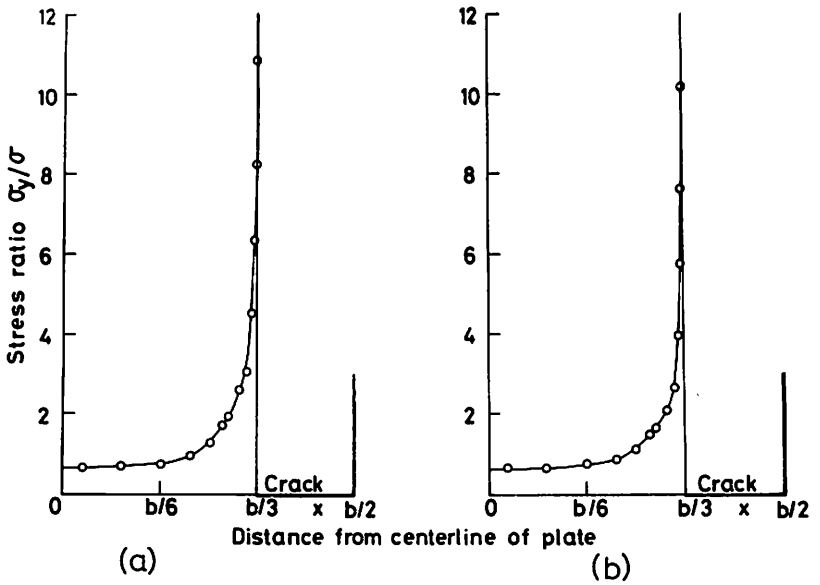

Fig. 10a Stress in plane z=0

Fig. 10b Stress in plane z=b/10

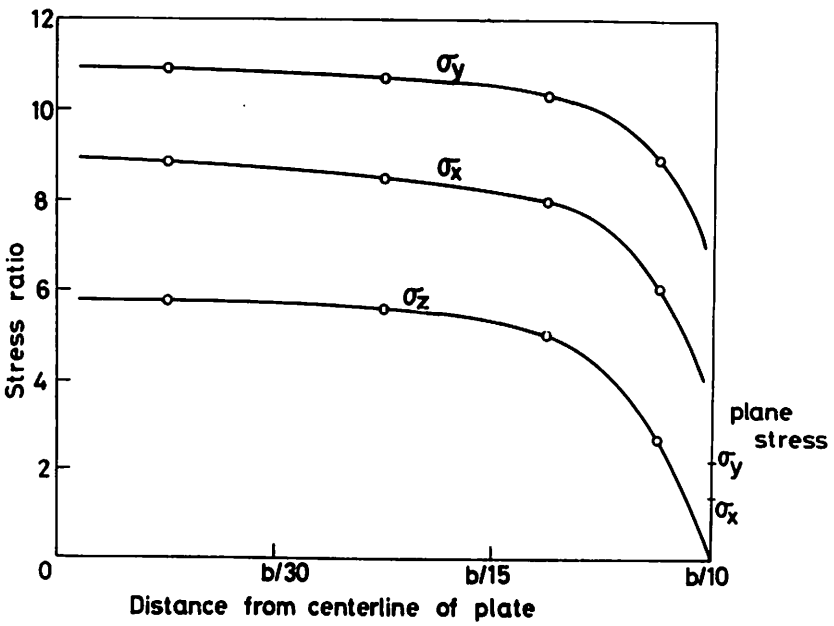

Fig. 11 Variation of ratio of stress ahead of crack to applied gross tension through thickness for rectangular crack example

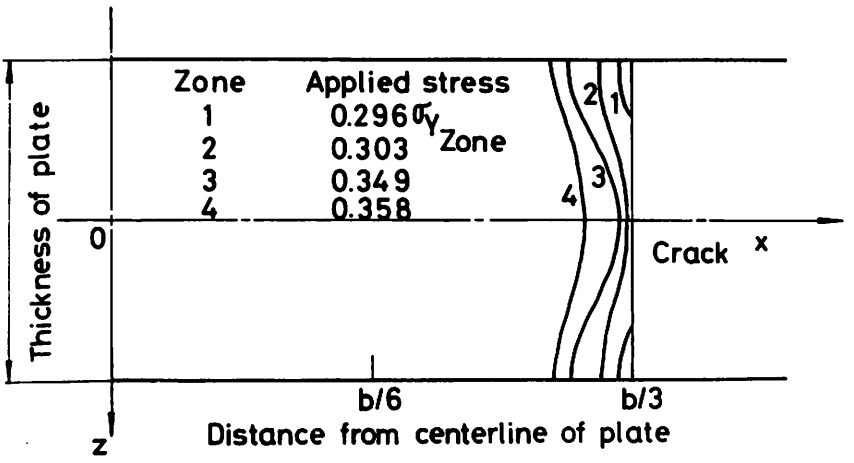

Fig. 12 Plastic zone size in plane of crack (y=0)

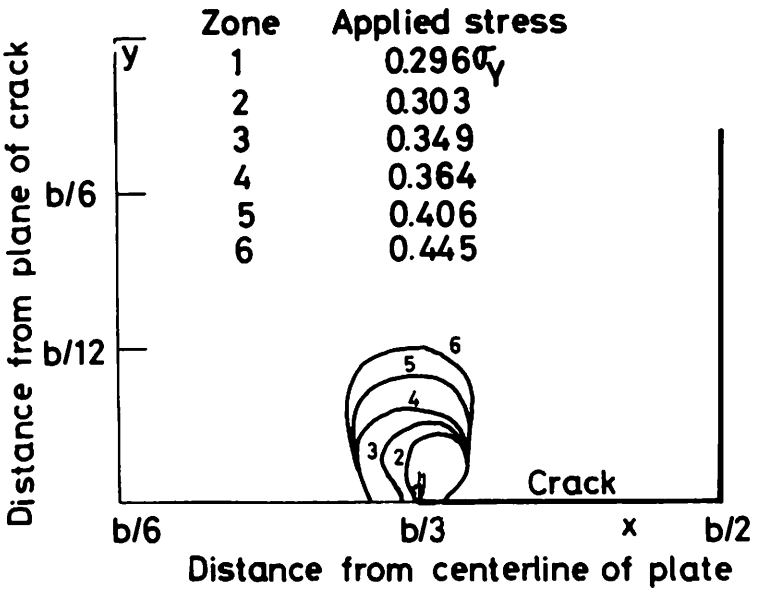

Fig. 13 Plastic zone size in plane z=0

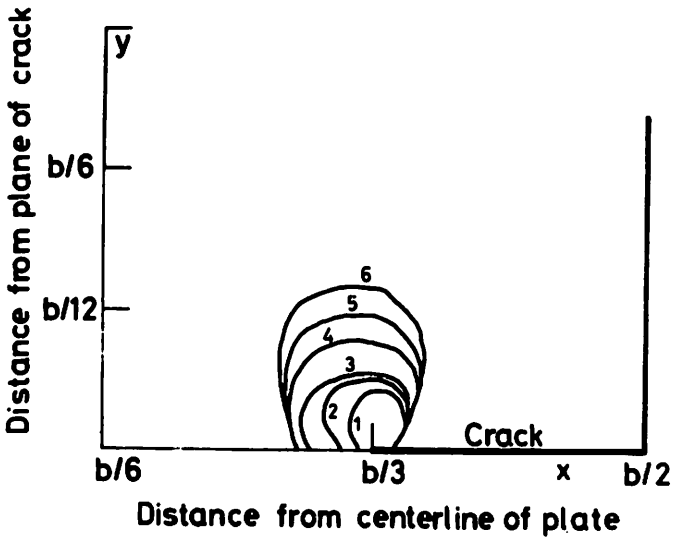

Fig. 14 Plastic zone size in plane z=b/10

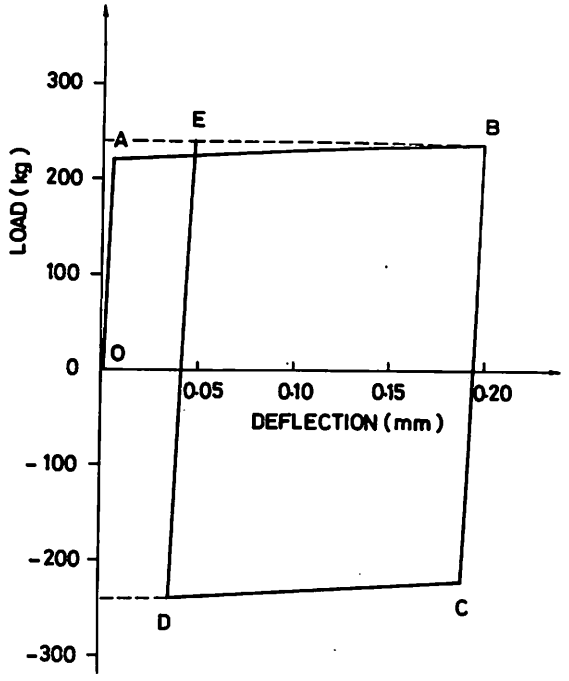

Fig. 15 The hysteresis curve of the test problem

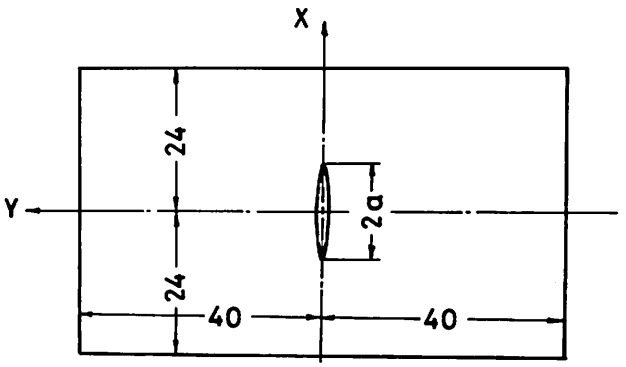

$\bar{\sigma} = \sigma_Y + H' \bar{\varepsilon}_p$
$E = 21000$ kg/mm^2
$H' = 57.0$ "
$\sigma_Y = 36.3$ "
$\nu = 0.3$

Fig. 16 The specimen with a centered crack

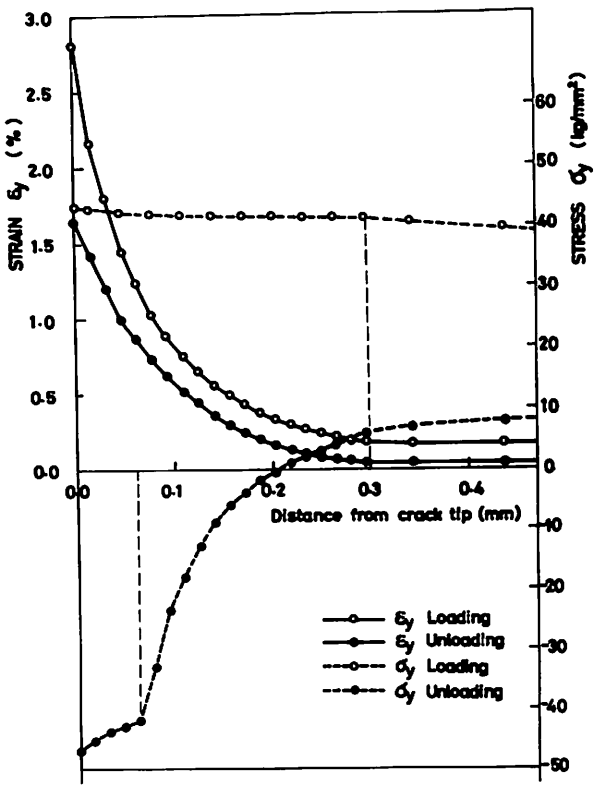

Fig. 17 The distribution of σ_y and ε_y ahead of the crack tip

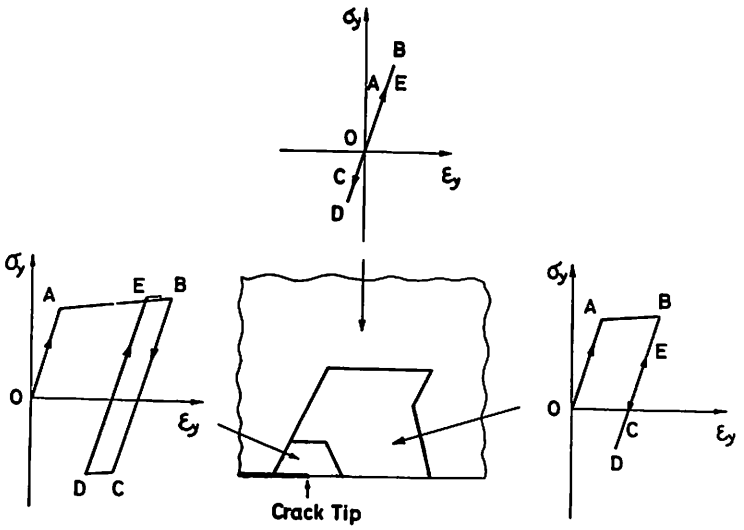

Fig. 18 Three domains near the crack tip

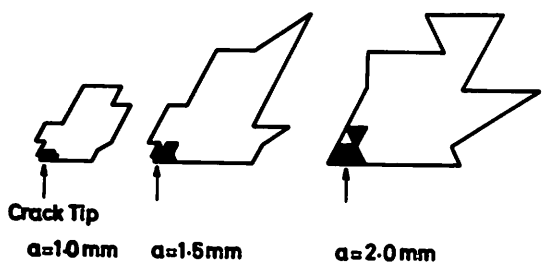

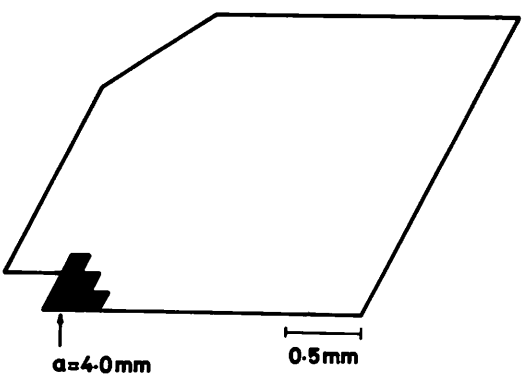

Fig. 19 The change in plastic zone

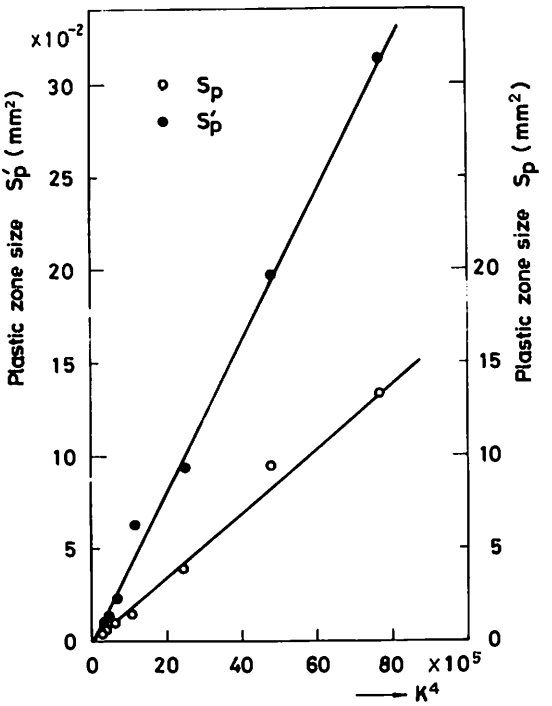

Fig. 20 The area of the plastic zone at peak load S_p and at zero load S'_p vs. K^4

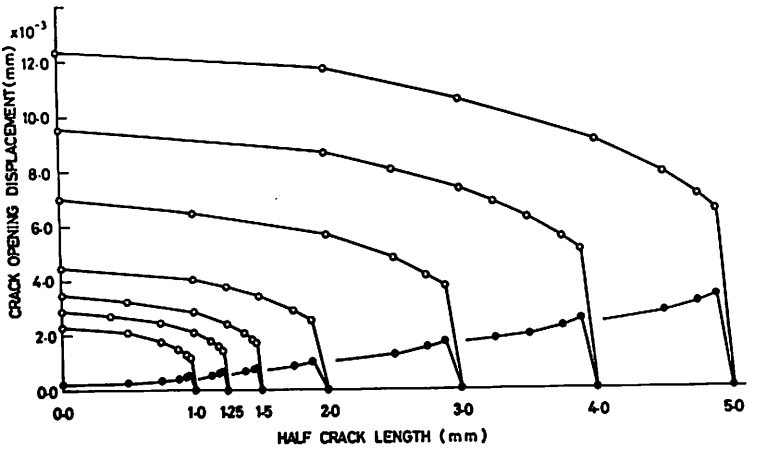

Fig. 21 The crack opening displacement

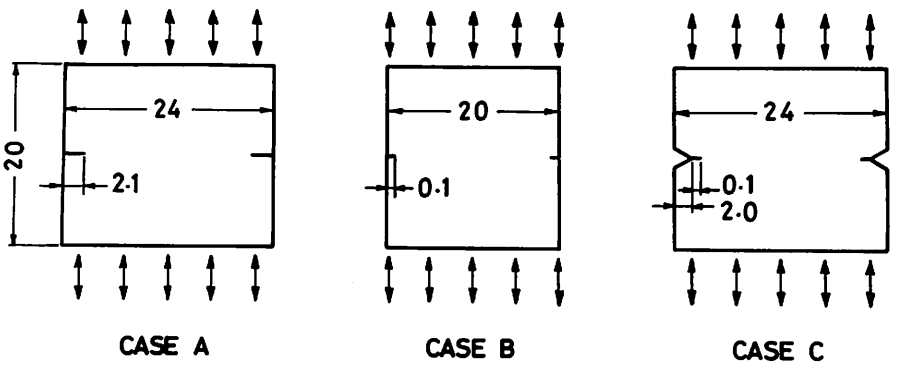

Fig. 22 The shape of the specimen

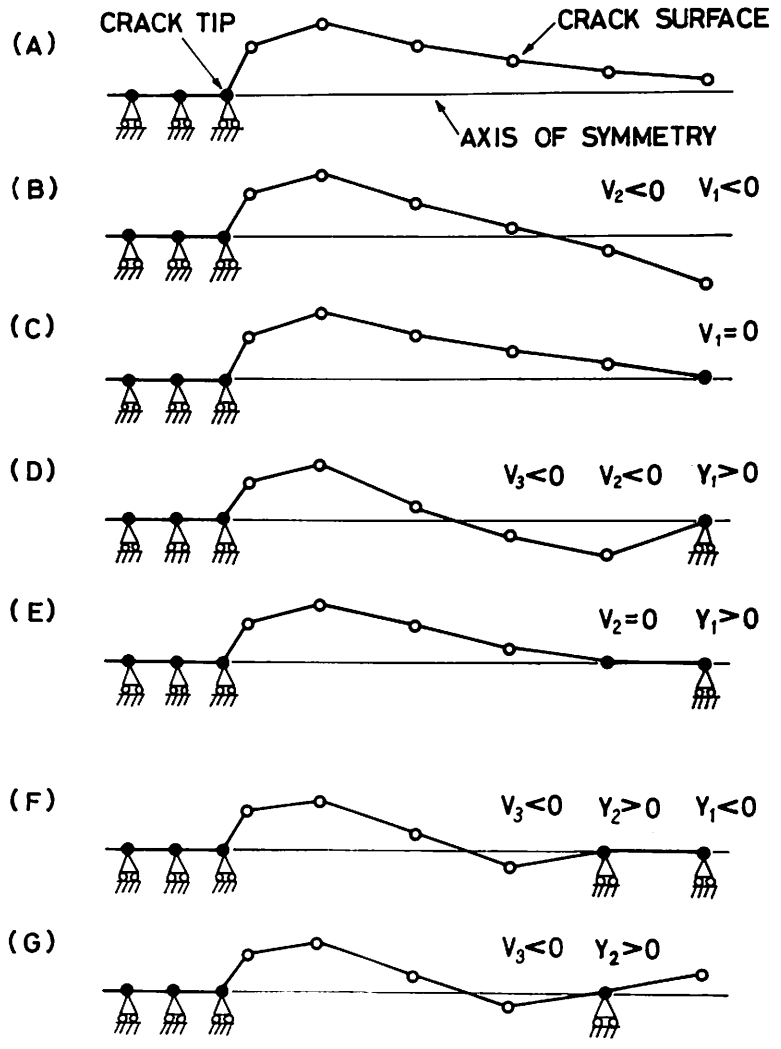

Fig. 23a The treatment of the boundary conditions on the crack surface

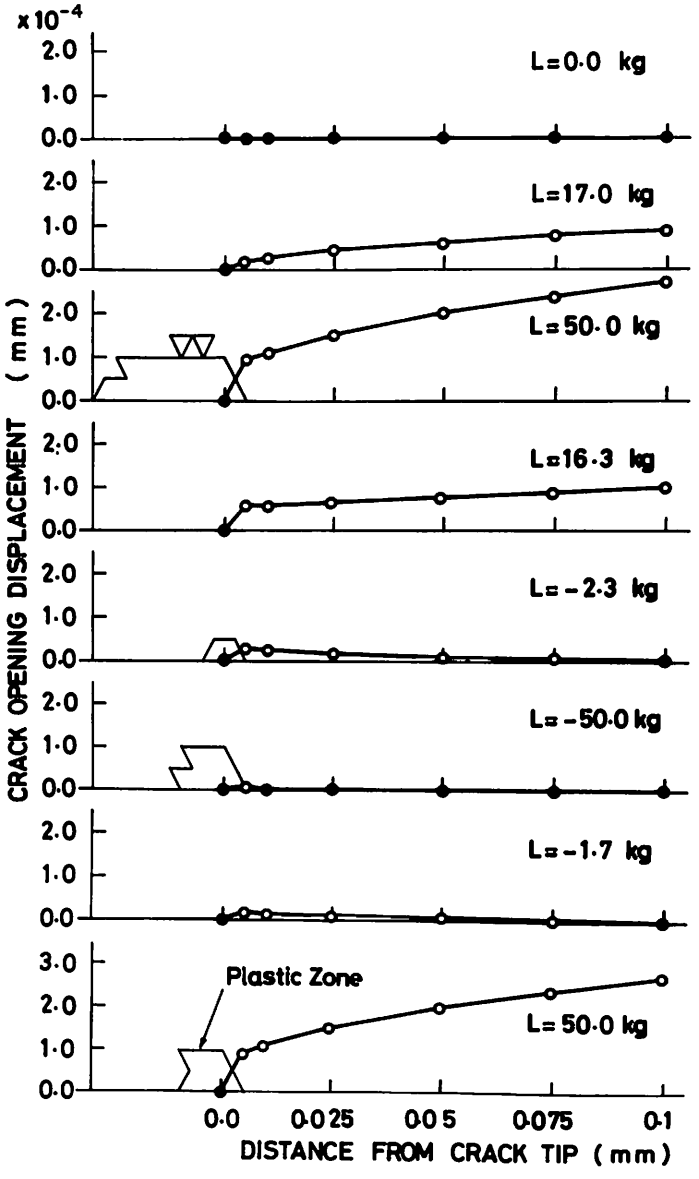

Fig. 23b The change in crack surface and plastic zone against the loading cycle

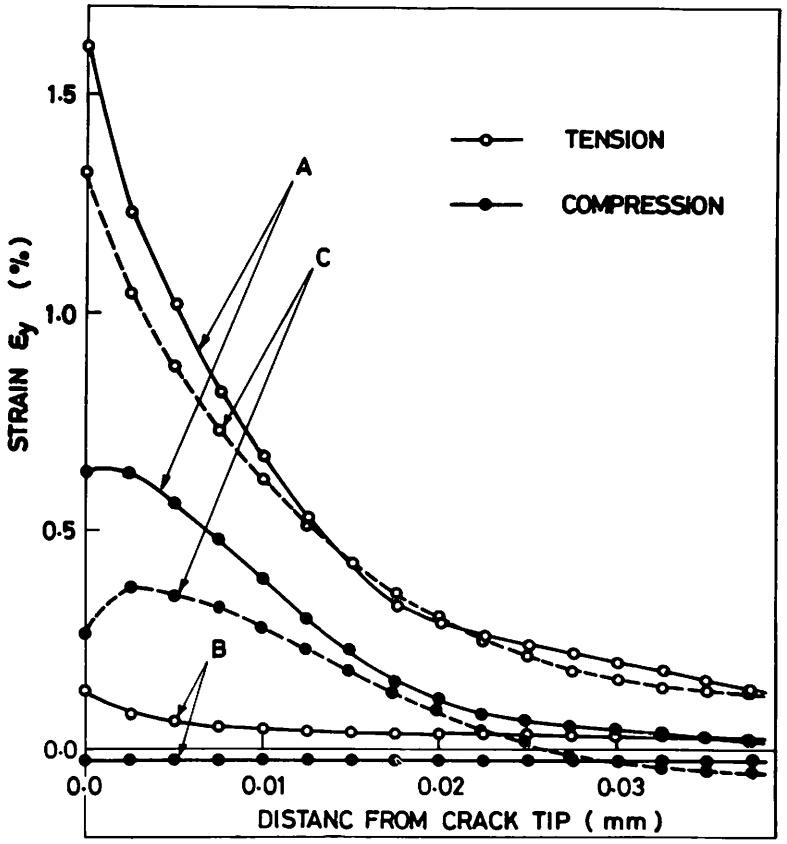

Fig. 24 The distribution of ε_y ahead of the crack tip in the case of a A, B, and C

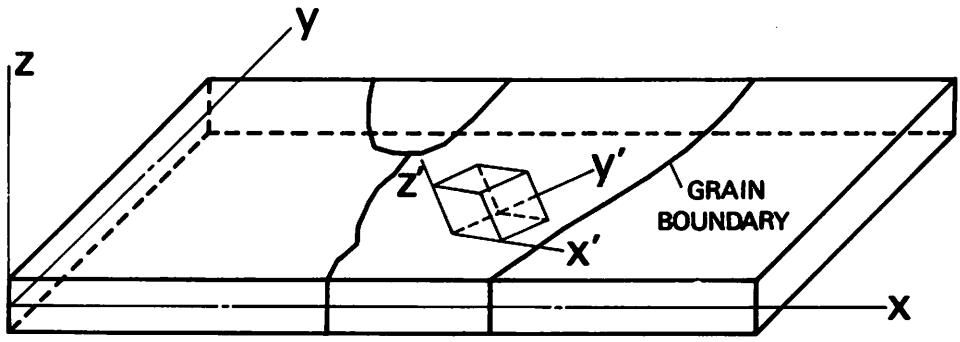

Fig. 25 Co-ordinate system

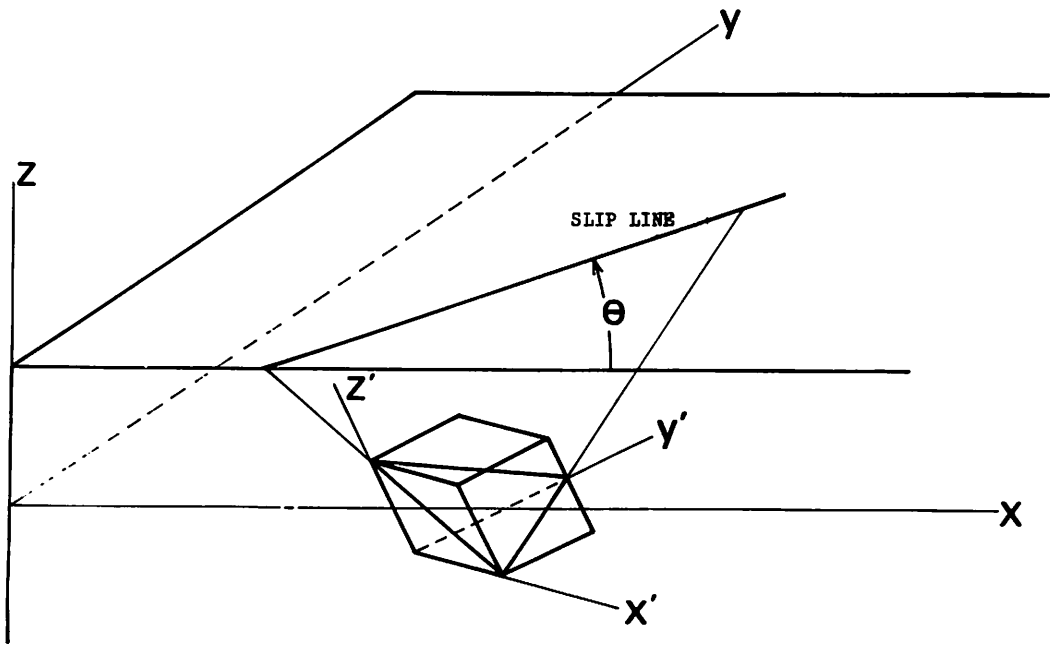

Fig. 26 Angle between the x axis and the slip line

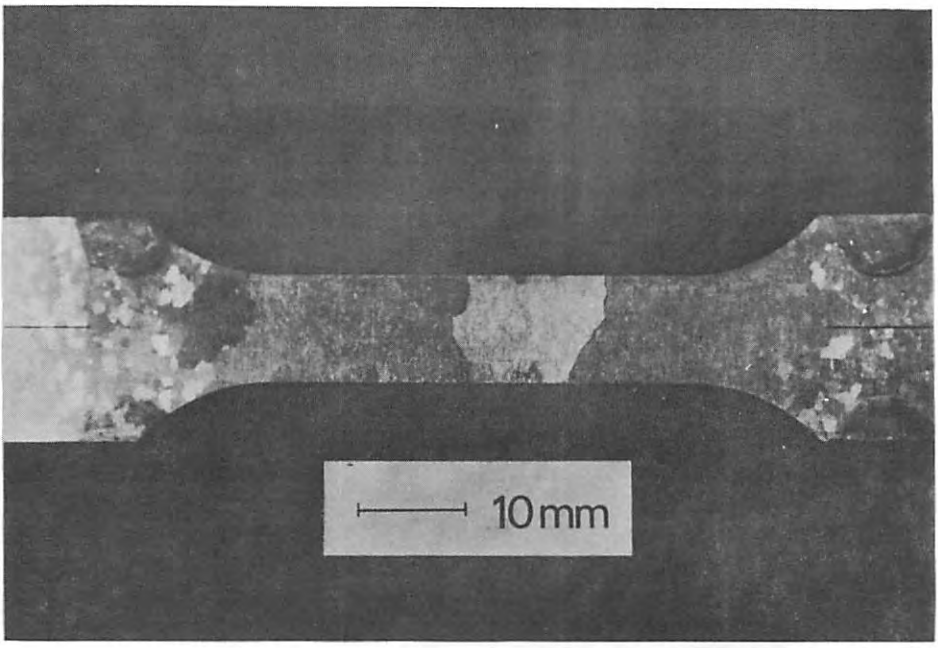

Fig. 27 Photograph of the specimen

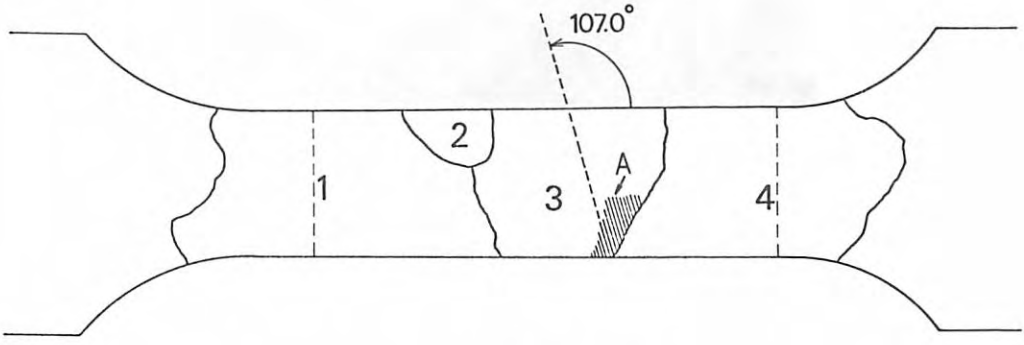

Fig. 28 Sketch of the specimen

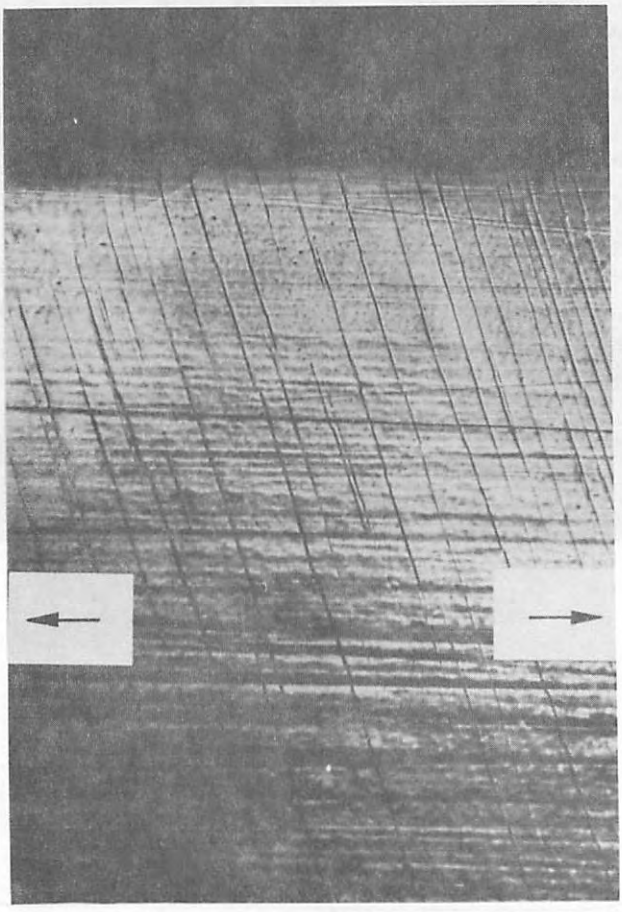

Fig. 29 Photograph of the slip line

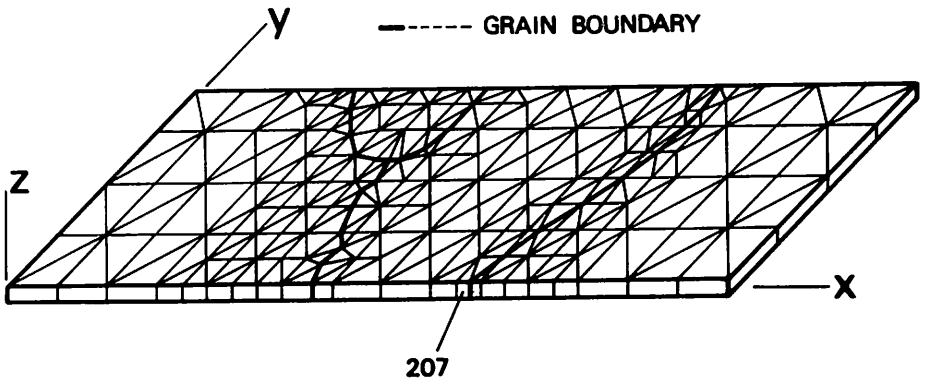

Fig. 30 Specimen divided into triangular prism elements

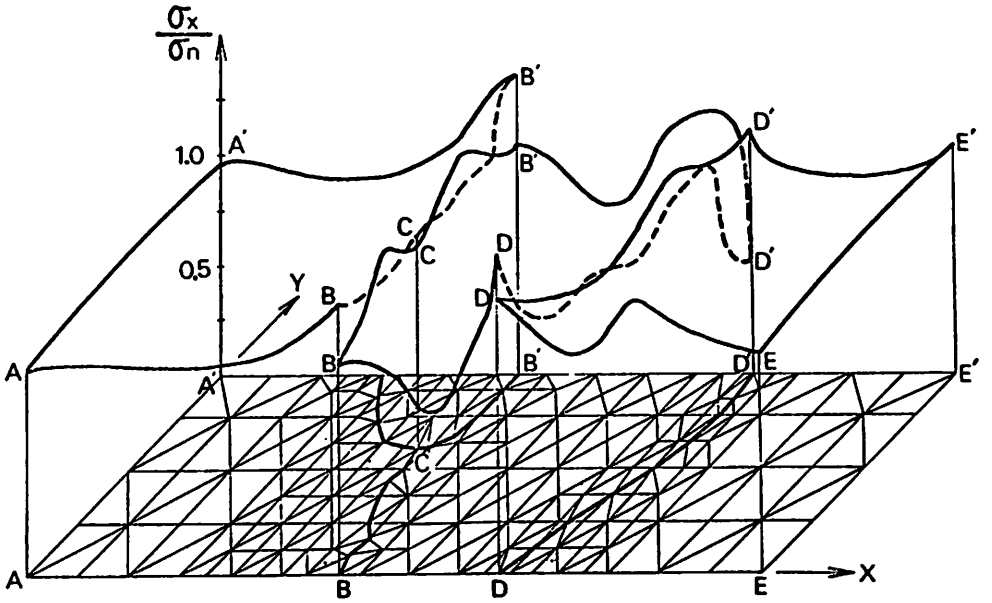

Fig. 31 Distribution of the stress σ_x

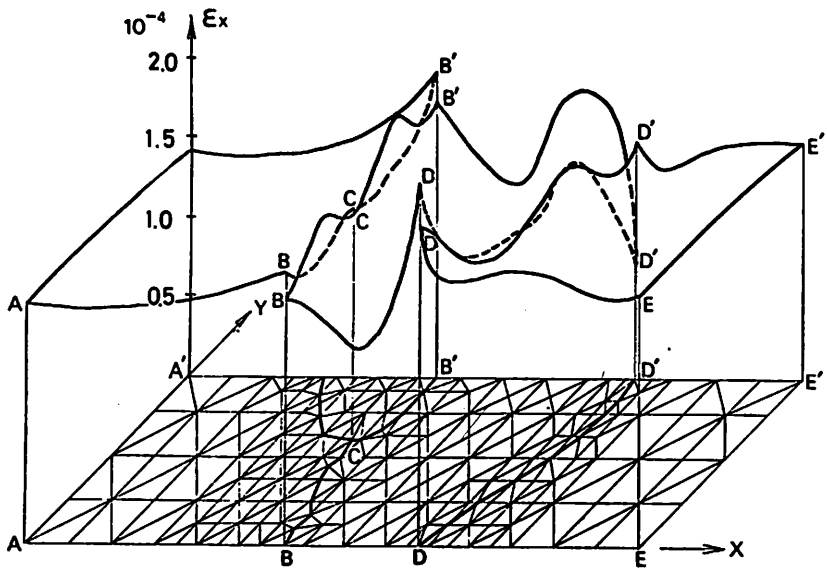

Fig. 32 Distribution of the strain ε_x (σ_n= 1.15 Kg/mm^2)

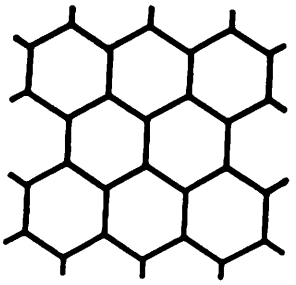

Fig. 33 A model of polycrystalline metal represented by hexagonal cylinders

Fig. 34 A hexagonal cylinder composed of six triangular cylinders

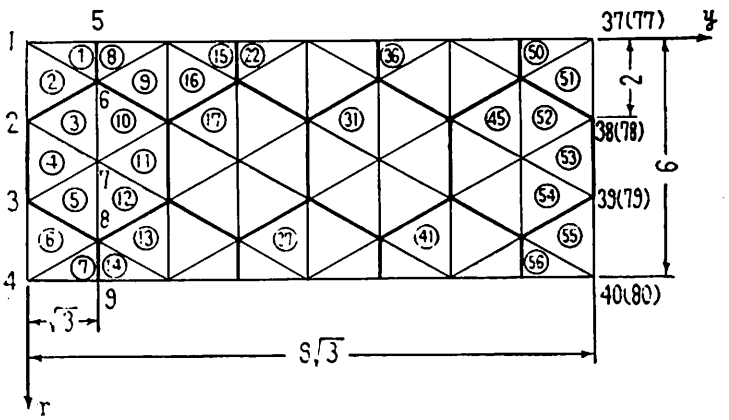

Fig. 35 Finite element representation

DISCUSSION

Q R. W. NICHOLS, U. K.

Referring to your calculations of size of plastic zone with repeated loading, would it be possible to extend this to the calculation of crack opening displacement as it changes on reloading ? Such calculations could be very helpful to the assessment of the effects of over-stressing in the initial or repeat pressure tests in relation to reduced risk of fast fracture on subsequent loading to a lower load, and may help to define recommendable stress levels in such tests.

A H. MIYAMOTO, Japan

In my model I can show you the displacement if you give me the coordinates of the point. I show some results of crack opening displacement in Fig. 21 of my paper.
But my calculation is confined to a 2-dimensional problem, and the results depend on the character of the material, so it cannot be applied at once to the practical problem.
If you give me some data, that is the stress-strain curve, the dimension of T. P., the amplitude of the cyclic loading, I will try to calculate it.

Q J. W. SPRETNAK, U. S. A.

In your calculations on the plastic zone in completely reversed fatigue loading, the plastic zone is decreased. Do you have data on the total plastic strain at the crack tip after the cycle ?

A H. MIYAMOTO, Japan

I left the data in Japan, so I cannot answer here. Afterwards I will send you my data.